

Mono-polar clustering of self-propelled particles through left-right asymmetry

Tetsuya Hiraiwa^a ^{1,2,*} Ryo Akiyama^a ³ Daisuke Inoue, ⁴ and Arif Md. Rashedul Kabir, Akira Kakugo⁵

¹*Mechanobiology Institute, National University of Singapore, Singapore 117411, Singapore*

²*Universal Biology Institute, The University of Tokyo, Hongo, Tokyo 113-0033, Japan.*

³*Department of Chemistry, Kyushu University, Fukuoka 819-0395, Japan*

⁴*Faculty of Design, Kyushu University, Fukuoka 815-0032, Japan*

⁵*Faculty of Science, Hokkaido University, Sapporo 060-0810, Japan*

(Dated: February 28, 2025)

Self-propelled particles form various patterns through dynamic self-organization like swarming. Here, we explore numerically a new mechanism of mono-polar clustering of self-propelled particles by controlling left-right asymmetry of motility with bidirectional alignment. We apply two types of torque to the particles, resulting in rotation of global orientation and clustering depending on the balance of the two torque. The particles in global orientation exhibit bi-polar motion, while the clusters predominantly exhibit mono-polar motion. This mono-polar cluster actually recapitulates the rotating swarms observed in a microtubule gliding assay.

^a TH and RA equally contributed to this work. TH proposed the model and performed the numerical simulations, and RA interpreted the results and constructed the logic.

* mbithi@nus.edu.sg

I. INTRODUCTION

Collective motion is an emergent phenomenon exhibited by living organisms, which gives rise to fascinating patterns [1–3]. Recently, the collective motion and patterns observed in nature have been contemplated in artificial systems by using the cytoskeletal filaments microtubules (MTs) and F-actins. Upon propulsion by their associated bimolecular motors, cytoskeletal filaments exhibited collective motion mediated by attractive interaction [4–9] or crowded conditions [10–12]. Local alignment interactions, *i.e.* collision-induced alignment of two self-propelled filaments play important roles in the emergence of their collective motion [10–12]. The resulting patterns of circular mesoscopic structures, streams and vortices exhibited local or global rotational motion along clockwise (CW) or counterclockwise (CCW) direction [6–9, 12, 13] that resembled the coherent motion of living organisms *e.g.* bacteria [14, 15], fishes [16] and sperm [17].

In nature, rotational force/torque of dynamic protein filaments is known to play an important role in chiral morphogenesis of cells, tissues and organisms [18–20]. Similarly, in the artificial systems made of cytoskeletal proteins, chiral collective behaviors have been often observed [6, 7, 9, 12, 13, 21] as well as shown in Fig. 2(b) later. However, the relevance of chirality of individual elements to their collective behavior has remained elusive.

Being inspired by these facts, we have demonstrated an in-silico study on collective motion of self-propelled particles (SPPs) each of which has intrinsic chirality. In this study, we consider SPPs with intrinsic polarity where the SPP move on a two-dimensional substrate. The SPP interacts with each other through isotropic core repulsion and bi-directional alignment. Two types of torque, self-propelled torque (ST) and interaction torque (IT) (See Fig. 1 and Sect. II below for the detail), are applied to the particles as left-right (LR) asymmetric motility due to two-dimensionality. We have investigated the emergence of patterns by tuning the strength of ST and IT without manipulating their alignment interactions. We found that, a transition from homogeneous bi-polar to mono-polar clustering phases is obtained only through such LR asymmetry.

This preprint is organized as follows: Section II is devoted to explaining the numerical model and methods which we used for this study. In Sect. III, we demonstrate typical dynamics of this system induced by the above-mentioned two types of torque, ST and IT, and provide the phase diagram over ST and IT, which is followed by more detailed analyses. We summarize this study in Sect. IV.

II. MODEL AND METHODS

We consider N SPPs, which are located at $\mathbf{x}_j = (x_j, y_j)$ ($j = 1, 2, \dots, N$) and have intrinsic polarity $\mathbf{q}_j = (\cos \theta_j, \sin \theta_j)$ [23], in a regular rectangle space with periodic boundaries in two dimensions [13, 24–26]. We assume that locations and polarity directions of SPPs ($j = 1, 2, \dots, N$) obey

$$\Theta(\mathbf{q}_j) \frac{d\mathbf{x}_j}{dt} = v_0 \mathbf{q}_j + \mathbf{J}^{\text{VE}}_j \quad (1)$$

and

$$\frac{d\theta_j}{dt} = \mathbf{J}^{\text{AL}}_j \cdot \mathbf{q}_j^\perp + \xi + \omega^{\text{ST}} + \Omega^{\text{IT}}_j, \quad (2)$$

respectively, with $\mathbf{q}_j^\perp = (-\sin \theta_j, \cos \theta_j)$. Equation (1) assumes the over-damped dynamics, and each object moves along the polarity \mathbf{q}_j with a constant velocity v_0 [23] in the absence of volume exclusion interactions. SPPs mechanically interact with each other by the volume exclusion

$$\mathbf{J}^{\text{VE}}_j = \beta \sum_{j'(n,j)} \left(\frac{r}{|\Delta\mathbf{x}_{j,j'}|} - 1 \right) \frac{\Delta\mathbf{x}_{j,j'}}{|\Delta\mathbf{x}_{j,j'}|}. \quad (3)$$

The summation $\sum_{j'(n,j)}$ runs for all the neighbors j' of j -th SPP, defined by $|\Delta\mathbf{x}_{j,j'}| < r$ with $\Delta\mathbf{x}_{j,j'} = \mathbf{x}_j - \mathbf{x}_{j'}$. Equation (1) also assumes that each SPP hardly moves along the direction perpendicular to the polarity direction, using the rescaled anisotropic friction tensor $\Theta(\mathbf{q}_j) = \mathbf{q}_j \otimes \mathbf{q}_j + r_\zeta^{-1}(\mathbf{I} - \mathbf{q}_j \otimes \mathbf{q}_j)$ with the ratio $R_\zeta = \zeta_\parallel / \zeta_\perp$ of friction coefficients in parallel ζ_\parallel and perpendicular directions ζ_\perp [13]. (\otimes is the tensor product, and \mathbf{I} is the identity matrix.) Equation (2) assumes that polarity is spontaneously established for each SPP with a fixed amplitude, $|\mathbf{q}_i| = 1$, and only its direction can evolve over time [23]. The first term indicates bidirectional alignment interaction,

$$\mathbf{J}^{\text{AL}}_j = 2\alpha \sum_{j'(n,j)} (\mathbf{q}_j \cdot \mathbf{q}_{j'}) \mathbf{q}_{j'} \quad (4)$$

The coefficient α indicates the strength of alignment. The second term $\xi(t)$ represents Gaussian white noise with $\langle \xi_j \rangle = 0$ and $\langle \xi_i(t)\xi_j(t') \rangle = 2D\delta_{ij}\delta(t-t')$ with the statistical average $\langle \cdot \rangle$.

In this study, we also apply two different types of torque, self-propelled torque (ST) and interaction torque (IT), the particles, which are represented by the last two terms in Eq. (2). Reflecting the two-dimensionality, *i.e.* the fact that SPPs are gliding on the substrate so that the directionality in the z -axis exists, we assume torque as LR asymmetric motility (Fig. 1). In ST, we assume that intrinsic polarity \mathbf{q}_j of each SPP rotates with a given speed ω_{ST} in either CCW and CW direction. ω^{ST} denotes the strength of ST [Fig.1 left], which we assume is a given constant. It is to note that, ST has been observed in the *in vitro* gliding assay of MTs [6]. We further assume that, when SPPs collide, another torque is exerted on their intrinsic polarities which we name IT. Ω_j^{IT} denotes IT [Fig.1 right], given by $\Omega_j^{IT} = \omega^{IT}m_j$ with the number m_j of SPPs within the range r from the focused SPP and a constant ω^{IT} representing the strength of IT. Indeed, in an *in vitro* gliding assay of MTs on a kinesin coated surface, we observed the increasing mean curvature in a trajectory for increasing MT-density (data not shown [22]). In the absence of these LR asymmetries, this model is essentially the same as that given in Ref. [13].

We numerically calculate Eqs. (1)- (4), after non-dimensionalization with characteristic length $X \equiv r$ and time $T \equiv r/v_0$. (For these purposes, we can simply put $r = 1$ and $v_0 = 1$.) We apply the Heun's method with a discretized time step $dt = 0.004$ up to variable total steps M specified in each figure legend. The parameters are set $R_\zeta = 0.01$, $D = 0.01$, $\alpha = 1.0$ and $\beta = 0.1$ unless otherwise mentioned. The number of objects and the global object density are set to be $N = 20,000$ and $\rho = 0.2$, respectively, unless otherwise mentioned. The system size is $L = \sqrt{N/\rho}$ both for x and y .

III. RESULTS

A. Dynamics: Emergence of mono-polar clusters by interaction torque with bi-directional alignment

Typical snapshots are shown in Fig. 2. For a two-dimensional hard-disk system, formation of an ordered phase requires a packing fraction higher than 0.7 ($\rho = 0.89$) [27]. Despite a low global particle density ρ of 0.2, mono-polar motile clusters are observed in silico, as shown in Fig. 2(a). The clusters are caused by the CCW-IT ($\omega^{IT} = 0.001$, $\omega^{ST} = 0.000$). The largest cluster is found to be composed of several thousands of particles. Magnified time overlay images reveal the rotational motion of the clusters in the CCW direction [Fig. 2(a)-right]. While rotating, the clusters collide with each other and the particles scatter in all directions, which is followed by regeneration of the clusters. An experimental result, presented in Fig. 2(b), shows collective motion of MTs driven by kinesins. Although the density is low, MTs are found to align upon collision and form clusters that also rotate in the CCW direction [Fig. 2(b) (right)]. Thus, the experimental result seems to agree to that observed in our in silico investigation.

Next, we examine how torques affects this clustering. Figure 2(c) shows the gas-like phase, in which neither the collective motion, nor the clustering was observed. This suggests that motility ordering requires alignment interaction, which may effectively cause SPP-SPP attraction. By contrast, for ST-CCW ($\omega^{ST} = 0.002$), SPPs exhibit homogeneous bi-polar phase even for such low packing fraction [Fig. 2(d)]. The velocity vector of the magenta and green particles form an angle of π , which confirms motion in the opposite direction. Global orientation of SPPs rotated CCW [13, 21].

Here, we discuss breaking of isotropic nature of particle motion. Under weak noise, motile direction of SPP is almost unchanged except when the particles collide. In the early stages, the isotropy of the system fluctuates. We assume that the number of particles with motion in a certain direction increase a little by chance. The collision probability of the SPPs of this certain and opposite directional motion is smaller than that for the others. Upon collision, the direction of motion is changed. If the new direction is same to the certain and opposite direction, the collision probability becomes smaller and the direction is maintained. Repetition of such events eventually induces anisotropy. Thus, most particles tend to avoid collisions and the bi-polar phase emerges. When ST is exerted to the system, the bi-polar motion becomes biased and is rotated [Fig. 2(d)].

The increase of IT changes a stable state from bi-polar phase to the rotating mono-polar phase [Fig.2(a)]. Clustering is mediated by alignment interaction and IT. Although both the mono- and bi-polar orientation of motion can be stabilized by alignment interaction, simulations for a few SPPs in Fig. 3 reveal that, in the absence of IT, bi-polar orientation is stable and swarms rarely formed. In contrary, IT rotates motile directions of SPPs moving in the same direction as a cluster, which breaks bi-polar orientation [Fig. 3(a-c)]. For particles moving in the same direction, alignment interaction worked as an effective attractive interaction. Multiple collisions between a large number of particles enhanced this directional motion, resulting in a mono-polar phase. This effect disappeared within the directional relaxation time ($t = 100$) [Fig. 3(d)]. The clusters were maintained, when the mean collision time was smaller than the relaxation time.

B. Phase diagram

In Fig. 4, correlation of morphology (a, b), the number fraction of SPPs in mono-polar clusters (c, d), and the angular velocities(e, f) with ST and IT are shown. The structures formed through collective motion of SPPs is found dependent on both types of torque. From the time-overlay images, two distinct morphology, mono-polar clustering phase and bi-polar phase can be identified. The doughnut-like shapes, formed by the rotating clusters, represent the mono-polar phase. Some structures shown in fuzzy color in which rotating clusters were not observed represent stable bi-polar phase. For instance, rotating clusters are not observed when $\omega^{IT} = 0$. Since, the effective attraction between particles is generated by the IT and alignment interaction, these results seem reasonable. The bi-polar phase is observed for relatively high values of ω^{ST} and low values of ω^{IT} [Figs. 4(a,b)].

When the ST and IT were opposite to each other, we found an island region in the lower right of Fig.4(b) and (d) for the clusters rotating in the CW direction. The doughnut-like shapes in the island are the same as those in the mono-polar area on the upper left region in Fig. 4(d). However, the SPP number fraction in the polar order region of the island area is larger than that of the upper left region. Thus, the collision probability in the cluster increases and the density increases by the collisions as ω^{ST} becomes large. The density reaches the values in the case of the same direction [Fig. 4 (c)]. Therefore, the increase of the collision caused by the ST makes another mono-polar clustering phase appear.

As mentioned above, the rotating clusters are observed for high values of ω^{IT} [Fig. 4(a,b)]. As ω^{ST} increases, the boundary between the mono-polar clustering and homogeneous bi-polar phases moves upwards towards higher ω^{IT} . This means, ST suppresses the formation of rotating clusters, which is also supported by analysis of the SPP number fraction in mono-polar clusters. In case of the same direction [Fig. 4(c)], the boundary appears for $\omega^{ST} < 2.0 \times 10^{-2}$. In the case of opposing direction [Fig. 4(d)], the boundary becomes unclear when $\omega^{ST} > 1.0 \times 10^{-2}$ because of the existence of the exceptional region for the CW-rotating clusters.

The boundary between the two phases appears as a band that extends. The map in the band is speckled at the right side of the black lines, which suggests that the mono-polar clustering and homogeneous phases are bi-stable. The speckled band is also found in the map of angular velocity for the case of the same direction [Fig. 4(e)]. Similar to the fraction in mono-polar clusters, the angular velocity is relatively high in the mono-polar clustering phase [Fig. 4(c)]. On the other hand, in Fig. 4(f), the color bands are straight and parallel which indicated that the angular velocity is governed by the balance between ω^{IT} and ω^{ST} . Thus, the angular velocity and the phase behavior are not strongly correlated, when the ST and IT are opposite each other.

In the case of opposing direction [Fig. 4(f)], the ω^{IT} is positive(CCW) whereas the ω^{ST} is negative(CW). The white grids, shown by the gray dashed line, indicate that rotations are canceled each other. Furthermore, the slope of the line was roughly 0.3. We also evaluated mean contact number around each particle in mono-polar clusters $\langle m_i \rangle_{i \in \text{MPC}}$ in the numerical calculation, for the parameter window exhibiting the polar order, and it was around 2 to 5. Hence, the above slope agrees with the condition for vanishing torque, $\omega^{ST} + \omega^{IT} \langle m_i \rangle_{i \in \text{MPC}} \sim 0$. It is to note that, since the global particle density ρ has been set to be 0.2, this means the contact number and the slope are the consequence of clustering.

C. Nature of the transition between homogeneous orientation and clustering states

As mentioned above, the region along the right side of the black line indicates a bi-stable state, i.e. coexistence of mono-polar clustering and homogeneous bi-polar phase [Fig. 4(c)]. As the transition between the homogeneous bi-polar and the mono-polar clustering phases looks like a first-order phase transition, the hysteresis behaviors are analyzed. Representative hysteresis behavior with the change of torque is shown in Fig. 5(a) which shows transition similar to a first-order phase transition. The fluctuation of SPP fraction in mono-polar clusters for the blue curve is larger than that for the red curve. When ω^{IT} decreases, the clusters are collapsed and the fluctuation becomes larger than that for the reverse process corresponds to clustering.

Fig. 5(b) shows the correlation between local density in ROIs with high polar order ($R > R_{\text{th}} = 0.9$) and the average angular velocity of particles. Data points in the same direction (circle) are scattered in the area where the average angular velocity is positive. On the other hand, the data points in the opposite direction (diamond) are scattered in the area where the average angular velocity is smaller than 0.015. The data points can be divided into two groups. One corresponds to gas-like phase. The local density is about 0.2 which is the same as the system particle density because the clustering does not appear under the condition. The other group of data points corresponds to mono-polar clusters (The local density is larger than 0.4). There is a discontinuous gap between them, which is consistent with the existence of hysteresis shown in Fig. 5(a).

D. On high density of clustering state

In the case of the same direction in Fig. 5(b), the local density in mono-polar clusters is between 0.4 to 1.5 with the median of 1.0. When the density is 1.0, the packing is almost the closest. The density increase as the absolute value of the average angular velocity increases. This result suggests that the collisions generate the effective attraction and mono-polar clusters are maintained by the collisions.

The density increase as the absolute value of the mean rotation speed increases. The collision becomes more frequent and stronger as the torque becomes greater. We can regard that the effective attraction between the particles is strong under such conditions. In the case of the opposing direction, this feature is remarkable. Therefore, we find the density 2.5 or more. The large value suggests, the particles overlay each other due to the strong collision. Here, the red diamonds for the high-density clusters belong to the island region of mono-polar clusters in Fig. 4(b) and (d) because the red diamonds mean $\omega^{ST} > 1.5 \times 10^{-2}$. The strong collisions in the cluster caused by the CW-ST and the CCW-IT are confirmed in Fig. 5(b). These high-density clusters are clearly distinguished from the low-density gas-like phase.

IV. CONCLUSION

We have demonstrated an *in silico* study to investigate the role of self-propelled torque and interaction torque of self-propelled particles in their coherent dynamics and its chirality. By varying the magnitude of two types of torque, we have explored the transition between different forms of coherent dynamics that are manifested by mono-polar clustering and homogeneous bi-polar order. We found that an increase in interaction torque breaks homogeneous order and stabilize the clusters. When the self-propelled torque increases, homogeneous order appears but its orientation rotates. Our results clarify the role of torque of self-propelled elements in the emergence of their coherent dynamics, chiral motion, and phase transition. This work should contribute to a better understanding of the regulation of chirality in the motion of self-propelled elements.

ACKNOWLEDGMENTS

We thank S. Tanida and M. Sano for valuable comments in TH's previous works which help us design this work. This research was supported by Mechanobiology Institute, National University of Singapore, (to TH), the JSPS KAKENHI grant number JP16K17777, JP19K03764 (to TH), JP19H01863, JP19K03772, JP18K03555, JP16K05512 (to RA) and JP18H03673 (to AK), a Grant-in-Aid for Scientific Research on Innovative Areas "Molecular Engine" (JSPS KAKENHI Grant Number JP18H05423) and a Grant-in-Aid for JSPS Research Fellows (18F18323) (to AK), "Leading Initiative for Excellent Young Researchers (LEADER)" (JSPS Grant number RAHJ290002) (to DI), and New Energy and Industrial Technology Development Organization (NEDO) (JPNP20006) (to AK).

- [1] Tamás Vicsek and Anna Zafeiris. Collective motion. *Physics reports*, 517(3-4):71–140, 2012.
- [2] I. D. couzin and N. R. Franks. Self-organized lane formation and optimized traffic flow in army ants. *Proc. R. Soc. London, B*, 270:139–146, 2003.
- [3] J. K. Parrish, S. V. Viscido, and D. Grünbaum. Self-organized fish schools: an examination of emergent properties. *Biol. Bull.*, 202:296–305, 2002.
- [4] Henry Hess, John Clemmens, Christian Brunner, Robert Doot, Sheila Luna, Karl-Heinz Ernst, and Viola Vogel. Molecular self-assembly of "nanowires" and "nanospools" using active transport. *Nano Letters*, 5(4):629–633, 2005. PMID: 15826099.
- [5] Yoshiki Tamura, Ryuzo Kawamura, Kazuhiro Shikinaka, Akira Kakugo, Yoshihito Osada, Jian Ping Gong, and Hiroyuki Mayama. Dynamic self-organization and polymorphism of microtubule assembly through active interactions with kinesin. *Soft Matter*, 7:5654–5659, 2011.
- [6] Ryuzo Kawamura, Akira Kakugo, Kazuhiro Shikinaka, Yoshihito Osada, and Jian Ping Gong. Ring-shaped assembly of microtubules shows preferential counterclockwise motion. *Biomacromolecules*, 9(9):2277–2282, 2008. PMID: 18662029.
- [7] Akira Kakugo, Arif Md Rashedul Kabir, Natsuki Hosoda, Kazuhiro Shikinaka, and Jian Ping Gong. Controlled clockwise–counterclockwise motion of the ring-shaped microtubules assembly. *Biomacromolecules*, 12(10):3394–3399, 2011.
- [8] Shoki Wada, Arif Md. Rashedul Kabir, Masaki Ito, Daisuke Inoue, Kazuki Sada, and Akira Kakugo. Effect of length and rigidity of microtubules on the size of ring-shaped assemblies obtained through active self-organization. *Soft Matter*, 11:1151–1157, 2015.
- [9] Shoki Wada, Arif Md. Rashedul Kabir, Ryuzo Kawamura, Masaki Ito, Daisuke Inoue, Kazuki Sada, and Akira Kakugo. Controlling the bias of rotational motion of ring-shaped microtubule assembly. *Biomacromolecules*, 16(1):374–378, 2015. PMID: 25474594.

- [10] Volker Schaller, Christoph Weber, Christine Semmrich, Erwin Frey, and Andreas R Bausch. Polar patterns of driven filaments. *Nature*, 467(7311):73–77, 2010.
- [11] Daisuke Inoue, Bulbul Mahmot, Arif Md. Rashedul Kabir, Tamanna Ishrat Farhana, Kiyotaka Tokuraku, Kazuki Sada, Akihiko Konagaya, and Akira Kakugo. Depletion force induced collective motion of microtubules driven by kinesin. *Nanoscale*, 7:18054–18061, 2015.
- [12] Yutaka Sumino, Ken H Nagai, Yuji Shitaka, Dan Tanaka, Kenichi Yoshikawa, Hugues Chaté, and Kazuhiro Oiwa. Large-scale vortex lattice emerging from collectively moving microtubules. *Nature*, 483(7390):448–452, 2012.
- [13] Sakurako Tanida, Ken’ya Furuta, Kaori Nishikawa, Tetsuya Hiraiwa, Hiroaki Kojima, Kazuhiro Oiwa, and Masaki Sano. Gliding filament system giving both global orientational order and clusters in collective motion. *Physical Review E*, 101(3):032607, 2020.
- [14] E. Ben-Jacob, I. Cohen, A. Czirók, T. Vicsek, and D. L. Gunton. Chemomodulation of cellular movement, collective formation of vortices by swarming bacteria, and colonial development. *Physica A*, 238:181–197, 1997.
- [15] D. Nishiguchi, I. S. Aranson, A. Snezhko, and A. Sokolov. Engineering bacterial vortex lattice via direct laser lithography. *Nature Communications*, 9:4486, 2018.
- [16] Audrey Filella, Françoise Nadal, Clément Sire, Eva Kanso, and Christophe Eloy. Model of collective fish behavior with hydrodynamic interactions. *Phys. Rev. Lett.*, 120:198101, May 2018.
- [17] Adama Creppy, Olivier Praud, Xavier Druart, Philippa L. Kohnke, and Franck Plouraboué. Turbulence of swarming sperm. *Phys. Rev. E*, 92:032722, Sep 2015.
- [18] Sundar Ram Naganathan, Sebastian Fürthauer, Masatoshi Nishikawa, Frank Jülicher, and Stephan W Grill. Active torque generation by the actomyosin cell cortex drives left–right symmetry breaking. *eLife*, 3:e04165, 2014.
- [19] Yee Han Tee, Tom Shemesh, Visalatchi Thiagarajan, Rizal Fajar Hariadi, Karen L Anderson, Christopher Page, Niels Volkmann, Dorit Hanein, Sivaraj Sivaramakrishnan, Michael M Kozlov, et al. Cellular chirality arising from the self-organization of the actin cytoskeleton. *Nature cell biology*, 17(4):445–457, 2015.
- [20] M. Novak, B. Polak, J. Simunić, Z. Boban, B. Kuzmić, A. W. Thomae, I. M. ToliKuzmić, and N. Pavin. The mitotic spindle is chiral due to torques within microtubule bundles. *Nature Communications*, 9:3571, 2018.
- [21] Kyongwan Kim, Natsuhiko Yoshinaga, Sanjib Bhattacharyya, Hikaru Nakazawa, Mitsuo Umetsu, and Winfried Teizer. Large-scale chirality in an active layer of microtubules and kinesin motor proteins. *Soft Matter*, 14(17):3221–3231, 2018.
- [22] This may appear somewhere in future.
- [23] T. Hiraiwa, A. Nagamatsu, N. Akuzawa, M. Nishikawa, and T. Shibata. Relevance of intracellular polarity to accuracy of eukaryotic chemotaxis. *Physical Biology*, 11:056002, 2004.
- [24] T. Hiraiwa. Two types of exclusion interactions for self-propelled objects and collective motion induced by their combination. *Phys. Rev. E*, 99:012614, 2019.
- [25] T. Hiraiwa. Dynamical self-organization of idealized migrating cells by contact communication. *Phys. Rev. Lett.*, In press, 2020.
- [26] M. Hayakawa, T. Hiraiwa, Y. Wada, H. Kuwayama, and T. Shibata. Polar pattern formation induced by contact following locomotion in a multicellular system. *eLife*, 9:e53609, 2020.
- [27] E. P. Bernard and W. Krauth. Two-step melting in two dimensions: First-order liquid-hexatic transition. *Physical Review Letter*, 107:155704, 2011.

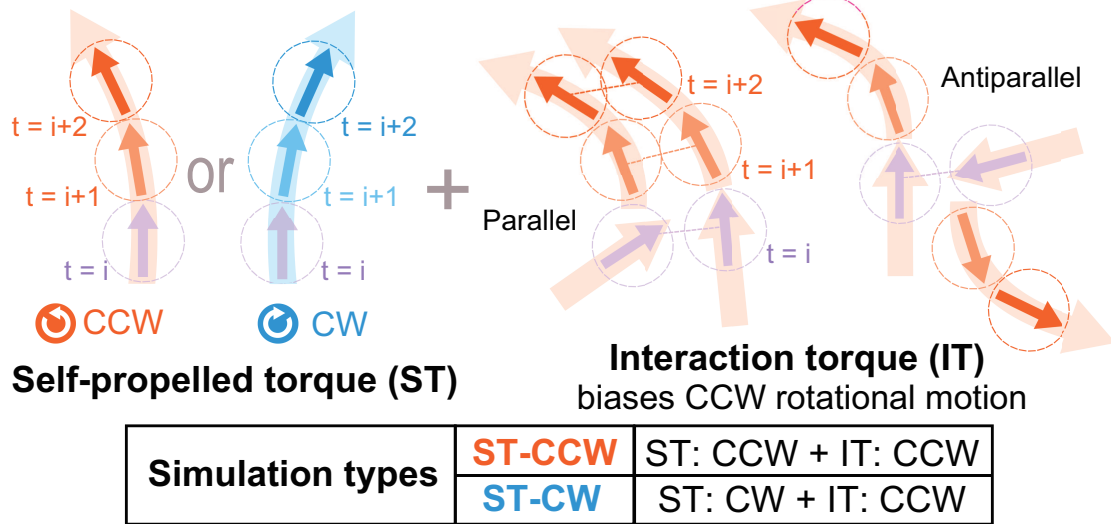


FIG. 1. Schematic diagrams show the application of self-propelled and interaction torque to SPPs.

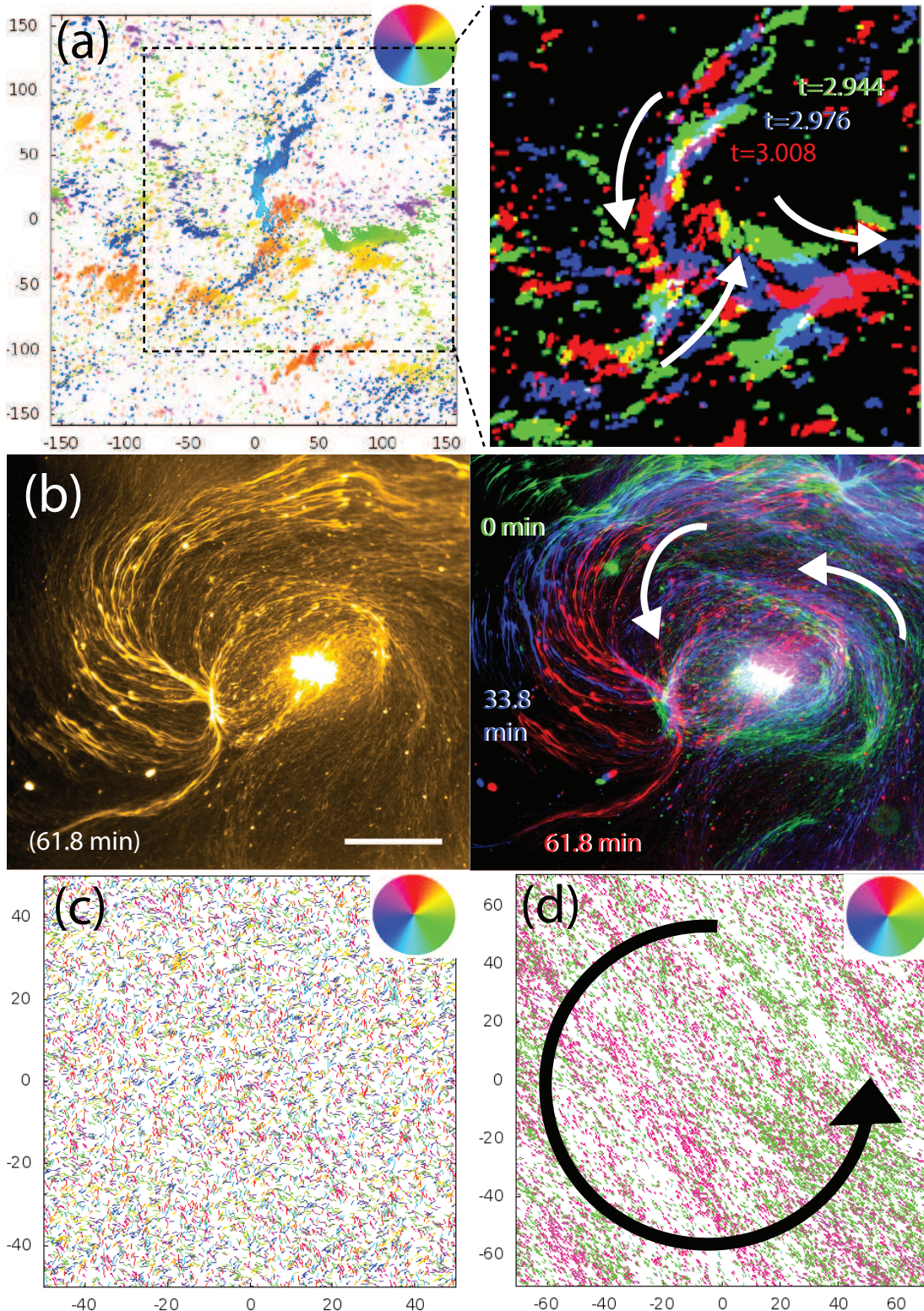


FIG. 2. Typical dynamic patterns observed in the numerical simulations and in vitro gliding assay of microtubules. See the text for details. (a) Mono-polar clustering; for $\omega^{IT} = 0.001$ and $\omega^{ST} = 0.0$. Right: Time overlay images show movement of clusters with time. [The green dots ($t=2.944$) have moved to the blue dots ($t=2.976$) and then to the red dots ($t=3.008$) (Fig. 2(a)-Right). The white arrows show the traveling motions]. Small structures have been removed by morphological erosion and dilation. (b) Mono-polar clustering of kinesin-driven microtubules in gliding assay and the corresponding time overlay image (right). Scale bar: $250\mu\text{m}$. The white arrows indicate the apparent motile directions of clusters in (a,b). (c) Image of a disordered phase; for $\alpha = 0.0$. While this snapshot is calculated for $\omega^{IT} = 0.0$ and $\omega^{ST} = 0.0$, the same disorder phase was obtained for any ω^{IT} and ω^{ST} as long as $\alpha = 0.0$. Other parameters are $N = 10,000$ and $\rho = 1.0$. (d) Image shows rotating global bidirectional ordered state; for $\omega^{IT} = 0.0$ and $\omega^{ST} = 0.002$ with $N = 20,000$. Black arrow indicates the rotation direction of orientation.

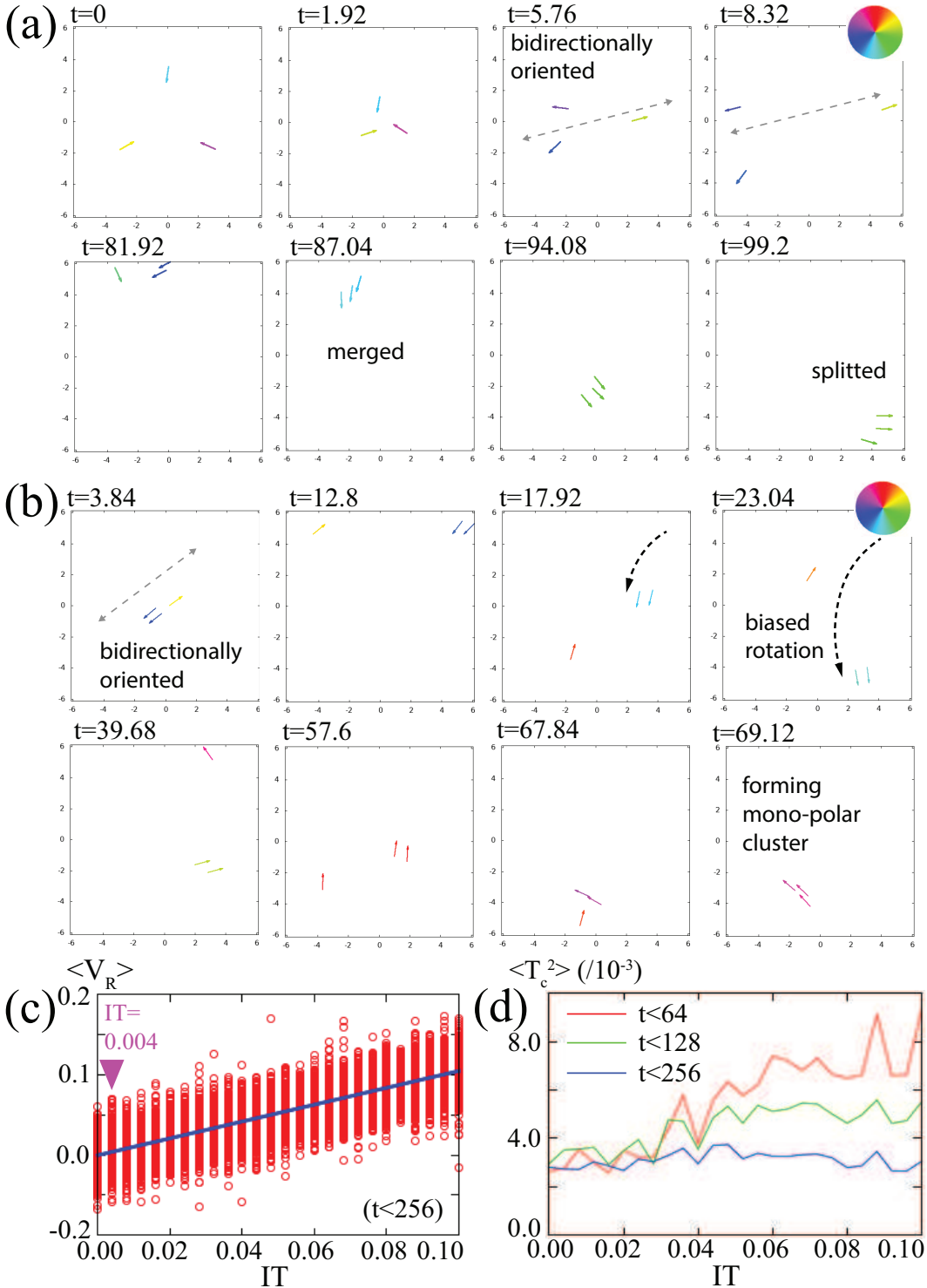
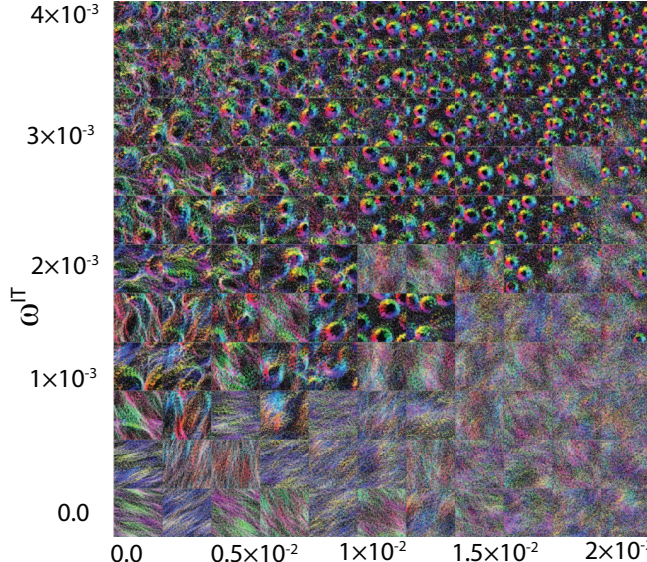
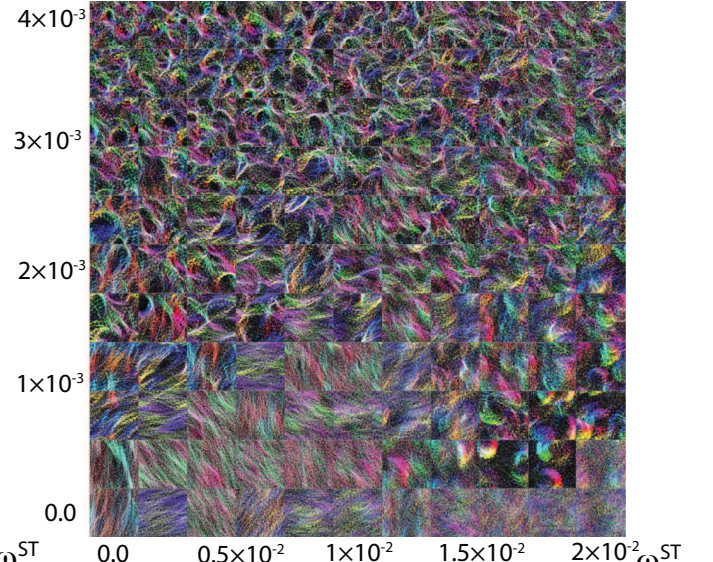


FIG. 3. Numerical simulations for dynamics of three particles in a regular square with periodic boundaries. (a) Snapshots for a single simulation. Each colored arrow represents the location and polarity direction of each element, and the color indicates its polarity direction corresponding to the color wheel. We here apply $IT = 0.1$, which is much larger than the maximum strength used in the main text, $IT = 0.004$, $ST = 0.0$, and the other parameters are the same as in the main text. (b) Another sample with the same parameter values with (a). A two-particle cluster rotated, which broke the bidirectional orientation, and resulted in formation of the mono-polar cluster. (c) Rotation velocity V_R of intrinsic polarities during the particle-particle contact, averaged over all elements and time ($\langle \cdot \rangle$) vs IT . Different marks corresponding to different runs (2,048 runs in total for each IT). The plots are fitted by $\langle V_R \rangle = (1.048 \pm 0.002)IT + (-0.00016 \pm 0.00011)$. (d) Full-contact time T_c vs IT for various maximum observation time $T_M = 64, 128$ and 256 . T_c is measured as the duration when there are two or three contacts among three particles within the observation time (from $t = 0$ to T_M). We calculate its proportion in a entire observation time, $\hat{T}_c \equiv T_c/T_M$, and plot squared \hat{T}_c averaged over 2,048 runs for each IT .

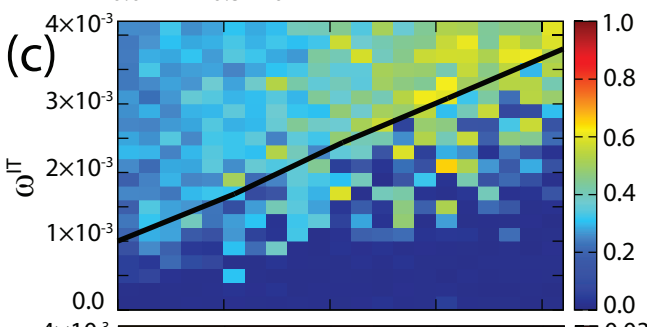
(a) Same direction



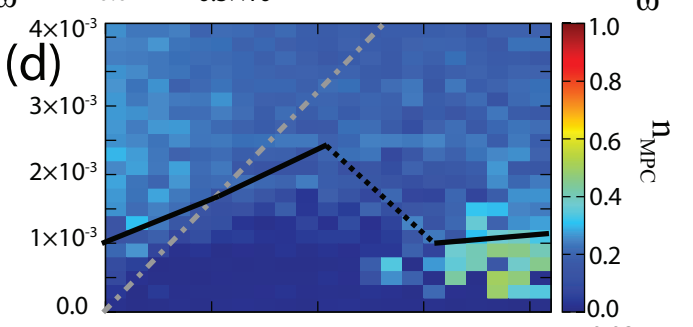
(b) Opposing direction



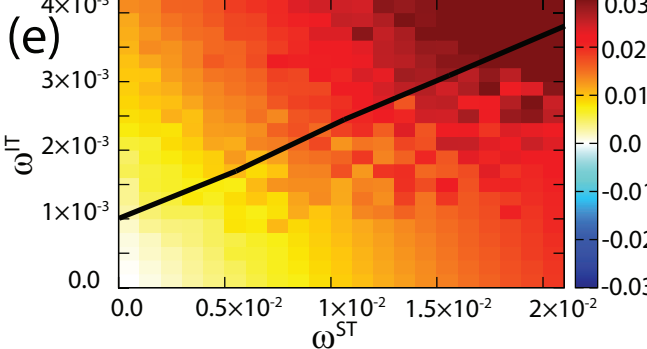
(c)



(d)



(e)



(f)

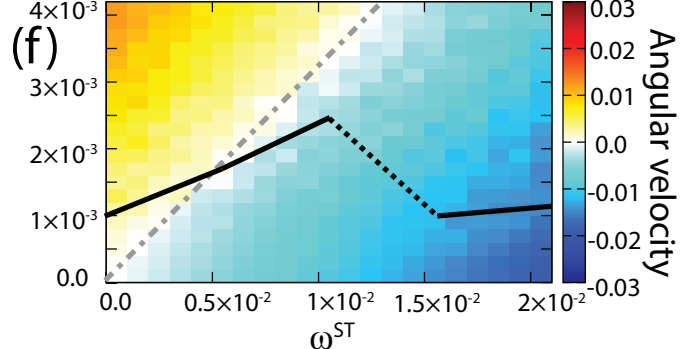


FIG. 4. Dependence of dynamic patterns on the torque strengths ω^{ST} and ω^{IT} . (a,b) Time-overlays. (c,d) SPP number fraction within mono-polar clusters n_{MPC} . To calculate, we first divide the system into 31×31 regions of interest (ROIs), and if a ROI has the polar order parameter R higher than $R_{th} = 0.9$, the ROI is regarded to be within mono-polar clusters. Giving the number of SPPs in all those ROIs N_{MPC} , the color axis shows $n_{MPC} = N_{MPC}/N$. (e,f) Average angular velocity of each SPP. ST's direction is set to be (a,c,e) the same as and (b,d,f) the opposite with IT's direction (CCW). Black curves indicate the stability limit of the global bi-polar order. Gray alternate long and short dashes lines highlight the parameters on which the angular velocity is zero.

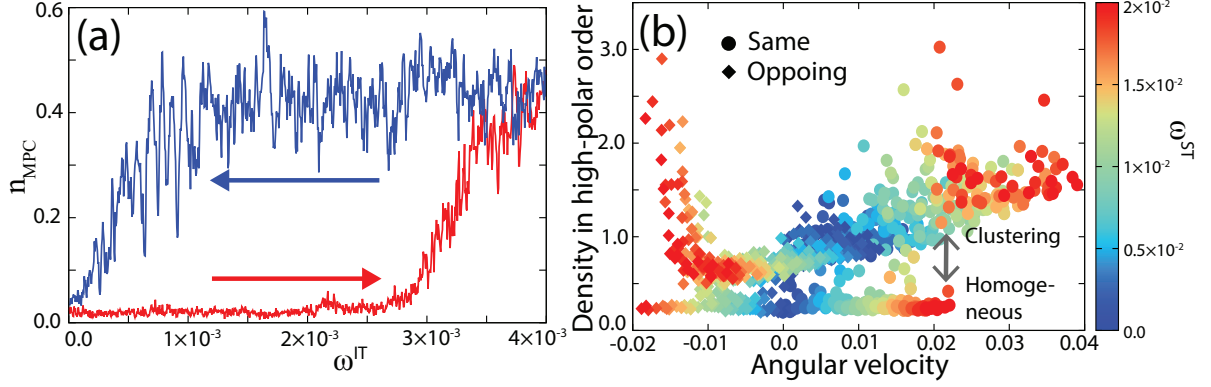


FIG. 5. First order transition-like behavior on mono-polar clustering. (a) Hysteresis of SPP number fraction in mono-polar clusters, n_{MPC} . ω^{ST} is set to be 0.01, and ω^{IT} was swept from 0 to 0.004 (ascent; red curve) and, after that, *vice versa* (descent; blue curve). See the legend of Fig. 4(c,d) for the definition of n_{MPC} . (b) Local density in regions with high polar order, against the average angular velocity of each SPP. The color of each mark indicates the IT strength ω^{ST} whereas the shape indicates the direction of ST (circles and diamonds; the same as and opposite to IT, respectively). Multiple marks with the same color and shape correspond to various ω^{IT} .